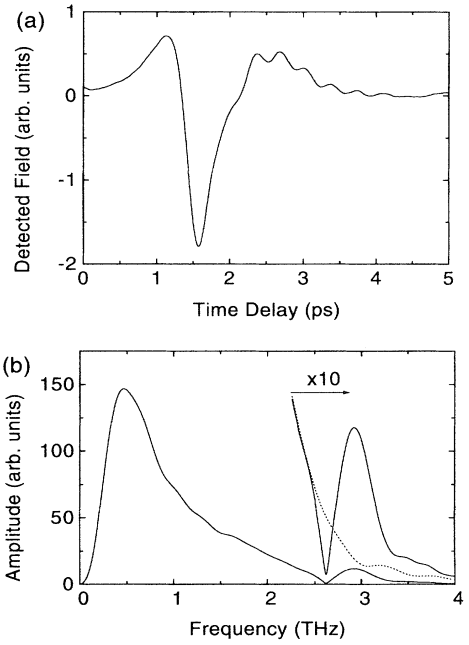

FIG. 3 (a) Detected electric field emitted from the $c\perp$ surface of Te. (b) Amplitude of the Fourier transform of the time-domain signal. The high frequency part is depicted also enlarged by a factor of 10. The dashed line gives the high frequency part of the antenna response determined from the emission of a broadband emitter (InP, also $\times 10$).

in electron and hole diffusion coefficients [14]. This effect is amplified by differences in the transient electron and hole temperatures. The screening of depletion-layer fields as the source of the radiation [5] can be neglected because the charged surface states have a low density and the band gap is small (0.33 eV) [6]. The amplitude of the initial THz signal due to the Dember field is only a factor of 5 weaker than the emission from a polar semiconductor with strong surface fields (e.g., InP) for the same excitation power. Figure 3(b) depicts the amplitude of the Fourier transform of the time-domain signal. The frequency spectrum reveals a broad peak at approximately 500 GHz. For high frequencies, the signal decreases to nearly zero at 2.62 THz before reaching a second maximum at about 2.9 THz. For clarity, this part of the spectrum is enlarged by a factor of 10. The high-frequency spectrum of a broadband emitting surface (InP, also $\times 10$, not normalized) is shown for comparison, representing the antenna response. The emission peak at 500 GHz results from the carrier transport dynamics leading to the buildup of the Dember field. The high-frequency features correspond to the oscillatory part of the time-domain signal. A strong deviation of the THz emission from Te compared to the broadband emitter is clearly observed in this frequency range.

The fact that the frequencies of two IR-active phonon modes (A_2 and E') overlap with the frequency range of interest, indicates that coherent phonons are the source of the oscillatory emission. Since the A_2 mode has an internal polarization perpendicular to the excited surface, while the E' mode is polarized parallel to the surface, a polarization-resolved analysis of the THz radiation allows the identification of the contributing modes.

Figure 4 depicts the THz signals emitted from the $c\perp$ surface with and without a wire-grid polarizer. The shift in the time delay results from the polarizer placed into the beam path of the THz radiation. The shape of the p-polarized THz radiation is similar to the radiation detected without polarizer. The oscillatory contribution remains clearly visible. The p-polarized emission originates from polarization changes perpendicular to the excited surface [5], i.e., the buildup of the longitudinal Dember field. In the s-polarized component, no contribution at phonon frequencies is observed and the signal shape has changed. The signal in this component must result from a different nonlinear polarization. Hence, the high-frequency oscillations in the THz emission result from an internal polarization *perpendicular* to the emitting surface, i.e., parallel to the c axis.

From these measurements we conclude that the A_2 mode dominates the high-frequency THz spectrum of the $c\perp$ surface. The E'_{TO} does not contribute, although it dominates the anisotropic RC in this frequency range. Thus we identify the dip at 2.6 THz in the spectrum of Fig. 3(b) with the $A_{2,\mathrm{TO}}$ mode, while the peak at 2.9 THz results from the $A_{2,\mathrm{LO}}$ mode being a strong source of radiation.

The emission of radiation from coherent phonons with polarization perpendicular to the excited surface is explained as follows: Coherent LO phonons are excited by the ultrafast buildup of a Dember electric field directed perpendicular to the excited surface. In contrast to the LO phonon generation via the ultrafast *screening* of surface fields in GaAs [1,8], Te LO phonons are driven by the *buildup* of a Dember field. The coherent LO phonons are associated with a macroscopic longitudinal polarization at the LO frequency emitting dipole radiation, which is detected in the far field by the antenna. The resonant

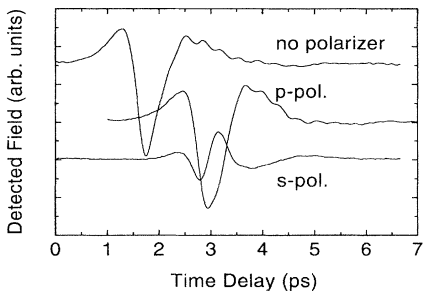

FIG. 4. THz field emitted from the $c\perp$ surface without polarizer and with polarizer placed before the antenna in p and s configuration. For clarity, the curves are shifted vertically.

coupling of the longitudinal Dember field with the LO phonon gives rise to an amplification of the field at the LO frequency and a strong reduction of the field at the TO frequency. Such effects have also been predicted for the case of THz emission by coherent LO phonons in GaAs [15]. We observe emission at the phonon frequencies and not at other frequencies from plasmon-phonon coupled modes [15], although the average plasmon frequency is close to the optical phonon frequencies. We explain the absence of plasmon-phonon coupled modes from the strong inhomogeneity of the carrier density resulting from the extremely short absorption length.

The above interpretation of THz emission by phonons is verified by excitation of the $c \parallel$ surface (not shown). The Fourier spectrum of the THz emission looks qualitatively the same as for the $c \perp$ surface. Now a dip in the spectrum is observed at 2.7 THz and a peak at 3.1 THz, which are close to the E'_{TO} and the E'_{LO} mode, respectively. In this case, the internal polarization of the observed phonon mode is again oriented perpendicular to the excited surface. At this surface, the Raman- and IR-active E'_{LO} is observed in both, the THz emission and the anisotropic RC. The E'' mode is not observed, as it is above the frequency detection limit and has only a weakly polar character.

Finally, we discuss the relevance of (i) propagation and (ii) out-coupling effects of the THz radiation. The buildup of the Dember field driving the coherent LO phonons is itself associated with the broadband emission of radiation. (i) The propagation of the transverse electromagnetic radiation at frequencies close to an optical-phonon resonance can also lead to a spectral modulation of the THz radiation [16]. This propagation effect can be neglected, since the thickness of the emitting region of approximately 30 nm is much shorter than the absorption length of the THz radiation, which is larger than 1 μm at the E'_{TO} frequency. (ii) The out coupling of the THz radiation from the crystal into air is influenced by the strong wavelength dependence of the refractive index at the phonon resonance. Assuming equal radiation intensities at the LO and TO phonon inside the crystal, impedance matching leads to a higher radiation intensity at the LO than at the TO frequency outside the crystal. However, calculations show that this effect by itself cannot explain the high electric field amplitude at the LO frequency and the total absence of radiation at the TO frequency observed in our experiments.

In conclusion, we report on the coherent excitation of optical phonons in single-crystal tellurium. All Raman-active phonon modes are observed in either the isotropic or the anisotropic time-resolved reflectivity changes in agreement with the symmetry of the Raman tensor. For the first time, we apply time-resolved THz emission spectroscopy for the investigation of coherent IR-active phonons. The THz emission by phonons of A_2 and E symmetry is observed. The observation of the emission of light from coherent phonons opens a new field in the investigation of lattice dynamics.

We gratefully acknowledge G. C. Cho and A. V. Kuznetsov for helpful discussions. This work was supported by the Alfried-Krupp Stiftung and the Deutsche Forschungsgemeinschaft.

[1] G. C. Cho, W. Kütt, and H. Kurz, Phys. Rev. Lett. **65**, 764 (1990).
[2] T. K. Cheng *et al.*, Appl. Phys. Lett. **57**, 1004 (1990); T. K. Cheng *et al.*, Appl. Phys. Lett. **59**, 1923 (1991).
[3] W. A. Kütt, W. Albrecht, and H, Kurz, IEEE J. Quantum. Electron. **QE-28**, 2434 (1992).
[4] H. J. Zeiger *et al.*, Phys. Rev. B **45**, 768 (1992).
[5] X.-C. Zhang and D. H. Auston, J. Appl. Phys. **71**, 326 (1992); H. G. Roskos, Lith. J. Phys. **34**, 175 (1994).
[6] P. Grosse, M. Lutz, and W. Richter, Solid State Commun. **5**, 99 (1967); P. Grosse, *The Physics of Tellurium,* Springer Tracts in Modern Physics Vol. 48 (Springer, Berlin, 1969).
[7] P. Grosse and W. Richter, in *Landolt-Börnstein, Numerical Data and Functional Relationships in Science and Technology,* edited by O. Madelung, Landolt-Bornstein, New Series, Vol. 17 (Springer, Berlin, 1983).
[8] T. Pfeifer *et al.*, Appl. Phys. A **55**, 482 (1992).
[9] For the anisotropic reflectivity measurement, only the polarizing beam splitter and a second photo diode are placed into the path of the reflected probe beam, leaving the excitation conditions unchanged.
[10] E modes with a scattering intensity only a factor of 5 smaller than that of the A_1 mode are observed in Raman spectra from the same sample. This difference between cw-Raman and time-resolved coherent-phonon experiments is a consequence of the displacive excitation mechanism (Refs. [2,4]).
[11] W. Richter, J. Phys. Chem. Solids **33**, 2123 (1972).
[12] A Ti:Sapphire laser instead of the CPM is used in the THz-emission experiments because of its much higher average power. The laser fluence at the sample is approximately the same for both experiments. The pump-probe experiments are also performed with a Ti:Sapphire laser at 1.7 eV energy, but the phonon amplitudes are higher for excitation with the CPM laser due to a broad resonance of the Raman process around 2.2 eV (Ref. [11]).
[13] H. Dember, Phys. Z. **32**, 554 (1931).
[14] The absorption length at 1.75 eV is approximately 35 nm [6], resulting in a large carrier gradient along the sample normal. Model calculation predicts the buildup of electric fields as large as 50 kV/cm immediately after excitation. The relevance of the Dember effect is supported by intensity-dependent measurements to be published elsewhere.
[15] A. V. Kuznetsov and C. J. Stanton (private communication).
[16] M. Born and K. Huang, *Dynamical Theory of Crystal Lattices* (Oxford University Press, Oxford, 1954).